FDG PET/CT Imaging 1 Week after a Single Dose of Pembrolizumab Predicts Treatment Response in Patients with Advanced Melanoma

Thomas M. Anderson[1], Bryan H. Chang[1], Alexander C. Huang[2,3,4,5], Xiaowei Xu[3,6], Daniel Yoon[2], Catherine G. Shang[1], Rosemarie Mick[3,5,7], Erin Schubert[1], Suzanne McGettigan[2,3], Kristin Kreider[2,3], Wei Xu[2,3], E. John Wherry[4,5,8], Lynn M. Schuchter[2,3], Ravi K. Amaravadi[2,3], Tara C. Mitchell[2,3], and Michael D. Farwell[1,3]

ABSTRACT

Purpose: Immunologic response to anti–programmed cell death protein 1 (PD-1) therapy can occur rapidly with T-cell responses detectable in as little as one week. Given that activated immune cells are FDG avid, we hypothesized that an early FDG PET/CT obtained approximately 1 week after starting pembrolizumab could be used to visualize a metabolic flare (MF), with increased tumor FDG activity due to infiltration by activated immune cells, or a metabolic response (MR), due to tumor cell death, that would predict response.

Patients and Methods: Nineteen patients with advanced melanoma scheduled to receive pembrolizumab were prospectively enrolled. FDG PET/CT imaging was performed at baseline and approximately 1 week after starting treatment. FDG PET/CT scans were evaluated for changes in maximum standardized uptake value (SUV_{max}) and thresholds were identified by ROC analysis; MF was defined as >70% increase in tumor SUV_{max}, and MR as >30% decrease in tumor SUV_{max}.

Results: An MF or MR was identified in 6 of 11 (55%) responders and 0 of 8 (0%) nonresponders, with an objective response rate (ORR) of 100% in the MF-MR group and an ORR of 38% in the stable metabolism (SM) group. An MF or MR was associated with T-cell reinvigoration in the peripheral blood and immune infiltration in the tumor. Overall survival at 3 years was 83% in the MF-MR group and 62% in the SM group. Median progression-free survival (PFS) was >38 months (median not reached) in the MF-MR group and 2.8 months (95% confidence interval, 0.3–5.2) in the SM group ($P = 0.017$).

Conclusions: Early FDG PET/CT can identify metabolic changes in melanoma metastases that are potentially predictive of response to pembrolizumab and significantly correlated with PFS.

Introduction

Cancer immunotherapy, including anti–programmed cell death protein 1 (anti–PD-1), anti–programmed death ligand 1 (anti–PD-L1), anti-CTLA-4, and anti-LAG-3 checkpoint blockade, has transformed the standard of care for many malignancies. Despite this success, many patients still do not respond, and immunotherapy can cause severe immune-related adverse events that can be permanent or fatal (1, 2). Thus, there is a need for noninvasive imaging biomarkers that can assess response early, to guide patient management and avoid toxicity in patients not likely to benefit.

^{18}F-fluorodeoxyglucose (FDG) PET/CT has the potential to noninvasively assess response early in the setting of cancer immunotherapy. Although FDG PET/CT is routinely used to detect metabolically active tumor cells, FDG is also taken up by a variety of activated immune cells from both the adaptive and innate immune system, which utilize aerobic glycolysis (also known as the Warburg effect) when they become activated (3). For example, *in vitro* studies have demonstrated markedly increased glucose uptake in activated T cells compared with unstimulated T cells, and preclinical studies have shown increased FDG uptake in tumor-associated myeloid immune cells, including macrophages, as well as activated T cells (4–7). In addition, clinical studies have demonstrated elevated FDG uptake in a variety of inflammatory conditions, including immune-related adverse events, and in ipsilateral regional lymph nodes following the flu or COVID vaccine (8–11).

In the routine clinical setting FDG activity in activated immune cells cannot be discriminated from FDG activity in tumor cells. However, if a baseline FDG PET/CT is compared with an early post-treatment FDG PET/CT over a short interval that minimizes tumor growth, changes in FDG uptake can be attributed to treatment-related effects, including increased FDG activity due to infiltration of the tumor by activated immune cells (metabolic flare) or decreased FDG activity due to tumor cell death (metabolic response). These metabolic changes, and in particular a metabolic flare, have been shown to reflect response in a preclinical mouse tumor model following treatment with immunotherapy (12), and in a few patients with metastatic melanoma

[1]Department of Radiology, Perelman School of Medicine, University of Pennsylvania, Philadelphia, Pennsylvania. [2]Department of Medicine, Perelman School of Medicine, University of Pennsylvania, Philadelphia, Pennsylvania. [3]Abramson Cancer Center, Perelman School of Medicine, University of Pennsylvania, Philadelphia, Pennsylvania. [4]Institute for Immunology, Perelman School of Medicine, University of Pennsylvania, Philadelphia, Pennsylvania. [5]Parker Institute for Cancer Immunotherapy at University of Pennsylvania, Philadelphia, Pennsylvania. [6]Department of Pathology and Laboratory Medicine, Perelman School of Medicine, University of Pennsylvania, Philadelphia, Pennsylvania. [7]Department of Biostatistics, Epidemiology and Informatics, Perelman School of Medicine, University of Pennsylvania, Philadelphia, Pennsylvania. [8]Department of Systems Pharmacology and Translational Therapeutics, Perelman School of Medicine, University of Pennsylvania, Philadelphia, Pennsylvania.

T.M. Anderson and B.H. Chang contributed equally to this article.

Corresponding Author: Michael D. Farwell, University of Pennsylvania, 3400 Spruce Street, Philadelphia, PA 19104. E-mail: michael.farwell@pennmedicine.upenn.edu

Clin Cancer Res 2024;XX:XX–XX

doi: 10.1158/1078-0432.CCR-23-2390

Translational Relevance

In this prospective pilot study, we demonstrated for the first time that metabolic changes in melanoma metastases on early FDG PET/CT are potentially predictive of response to pembrolizumab, and are correlated with progression-free survival. Given that FDG PET/CT is ubiquitous and routinely used to image patients with cancer, and changes in tumor SUV_{max} can be easily calculated, this approach has the potential to be readily applied to clinical practice. The early identification of nonresponding patients would allow treatment to be escalated, or alternative therapies to be given earlier, which could improve outcomes and reduce unnecessary side effects from ineffective therapy. In addition, the early identification of responding patients could enable de-escalation of therapy (and surgery), which could decrease morbidity and increase quality of life. This approach also has the potential to provide insight into the kinetics and heterogeneity of response to cancer immunotherapy, both between patients and between tumor lesions in the same patient.

treated with ipilimumab (13–16), and are potentially an earlier and more sensitive measure of response to cancer immunotherapy compared to anatomic imaging such as CT or MRI.

To capture tumor infiltration by activated immune cells, patients should ideally be imaged with FDG PET/CT near their peak immune response. Given that complete pathologic responses have been reported in patients with advanced melanoma 3 weeks after initiation of pembrolizumab, and robust increases in $Ki67^+$ CD8 T cells have been seen in the peripheral blood by 1 week, it is likely that the immune response to checkpoint blockade is quite rapid (17, 18). Thus, a prospective clinical trial was initiated to test the hypothesis that FDG PET/CT imaging performed at approximately 1 week after a single dose of pembrolizumab in patients with advanced melanoma would predict response to immunotherapy.

Patients and Methods

Patients

This prospective single-center study was approved by the Institutional Review Board at the University of Pennsylvania (ClinicalTrials.gov identifier NCT02791594). All patients provided written informed consent and the trial was conducted in accordance with the Declaration of Helsinki. Adult patients with advanced melanoma scheduled to initiate pembrolizumab were prospectively enrolled between November 2016 and November 2019. Patients were required to have at least 1 measurable lesion per RECIST 1.1. Patients could not have received previous anti–PD-1 or anti–PD-L1 therapies. Patients on systemic steroids or immunosuppression were not eligible, nor were patients with active brain metastasis. All patients were treated with pembrolizumab as a standard-of-care therapy (200 mg, i.v., every 3 weeks) in the first- or later line setting. FDG PET/CT imaging was performed within 4 weeks prior to initiation of pembrolizumab (PET0) and again at about 1 week after the first dose of pembrolizumab (PET1). Best response was assessed on standard-of-care imaging (CT, MRI, or FDG PET/CT) acquired at baseline and then every 3 months using RECIST 1.1 (19). Pathologic response was assessed for one patient, using the same methods described previously (17). An optional tumor biopsy was performed on the same date as the PET1 scan, after the scan was completed, if the biopsy could be obtained safely from an accessible site. Blood samples were collected at baseline (on the date of therapy initiation), on the same date as PET1, and at 3, 6, 9, and 12 weeks posttherapy.

FDG PET/CT imaging and analysis

FDG PET/CT scans were acquired according to a standard-of-care clinical protocol at the University of Pennsylvania using a Biograph mCT PET/CT scanner (Siemens), Biograph Vision PET/CT scanner (Siemens), Gemini PET/CT scanner (Phillips), and Ingenuity PET/CT scanner (Philips), which are routinely cross-calibrated by our medical physics group. CT images were obtained without intravenous contrast for attenuation correction and anatomic correlation. Patients were required to fast for 4 to 6 hours and have plasma glucose levels <200 mg/dL prior to injection of FDG. Patients were scanned supine from the vertex to the toes approximately 60 minutes after injection of 555 MBq (15 mCi) $\pm$ 20% of FDG. In patients with no lesions in the extremities, images were acquired from the base of the skull to the midthighs.

FDG PET/CT images were reviewed and analyzed using MIM (MIM Software) by one experienced physician board-certified in both diagnostic radiology and nuclear medicine who was blinded to patient outcome. Up to 5 RECIST-measurable lesions (2 per organ) were assessed for each patient. FDG activity for each lesion was measured using the maximum standardized uptake value (SUV_{max}), which was chosen because it is routinely used in clinical practice. The percentage change in SUV_{max} was defined as (sum of PET1 SUV_{max} – sum of PET0 SUV_{max})/(sum of PET0 SUV_{max}) $\times$ 100; the percentage change in lesion size was calculated similarly. The change in individual FDG-avid lesions was also assessed for exploratory purposes, with an FDG-avid lesion defined as focal, abnormally increased FDG uptake greater than background with a corresponding anatomic lesion on the CT scan suggestive of metastasis. Baseline tumor burden was calculated as the sum of the longest dimensions of all measurable baseline target lesions on the PET0 scan as assessed per RECIST 1.1 modified to include a maximum of 10 target lesions in total or five per organ, as described previously (20).

Sample processing: PBMCs and tumor

Blood samples were drawn in sodium heparin tubes, kept at room temperature, and processed within 8 hours of blood draw. Whole blood was centrifuged and plasma samples were collected, aliquoted in the volume of 1 mL per cryotube, and stored at -80°C. Blood samples were reconstituted by adding an equal volume of Hank's balanced salt solution (HBSS, Corning MT21021CM) to the volume of collected plasma. Reconstituted blood samples were diluted two-fold in HBSS and Ficoll (Ficoll-Paque PLUS density gradient medium, GE Healthcare Life Sciences, 17–1440–03) was layered underneath. The volume of Ficoll-Paque PLUS used was equal to that of the undiluted blood sample. The buffy coat was collected and washed twice with HBSS. Ammonium-chloride-potassium lysis buffer (Lonza 10–548E) was used to lyse the red blood cells, if necessary. Tumor biopsies were processed in the Department of Pathology and Laboratory Medicine, Hospital of the University of Pennsylvania, and immediately snap or formalin fixed and paraffin embedded; a portion of unfixed tissue was allocated for extraction of tumor-infiltrating lymphocytes (TILs), which was processed within 4 hours after excision from the patient. The unfixed tumor samples were cut into 2–3-mm pieces with a scalpel in an RPMI1640 (Corning 10–040-CM)-containing petri dish. A 70-μm cell strainer (Falcon 352350) was placed on top of a 50-mL conical tube and the tissue fragments were transferred to the cell strainer with a pipette. The cells were released by gently grinding the

tissue fragments using the thumb depressor of a sterile syringe plunger placed against the cell strainer. Cells were washed twice and counted in a hemocytometer. The numbers of lymphocytes and melanoma cells were distinguished by their morphology and recorded separately.

Flow cytometry

PBMCs and tumor suspension were stained with a master mix of antibodies for surface stains including CD4 (clone OKT4, BioLegend, RRID:AB_2563242), CD8 (clone RPA-T8, BD Biosciences, RRID:AB_2744460), CD45RA (clone HI100, BioLegend, RRID:AB_2563814), Tim-3 (clone F38–2E2, BioLegend, RRID:AB_11218598), Lag3 (clone 3DS223H, eBioscience, RRID:AB_2574048), CD39 (clone A1, BioLegend, RRID:AB_940425), CD38 (clone HIT2, BD Biosciences, RRID:AB_2738515), KLRG1 (clone SA231A2, BioLegend, RRID:AB_2566595), CD27 (clone L128, BD Biosciences, RRID:AB_2744350), and PD-1 (clone EH12.1, BD Biosciences, RRID:AB_2739514) and intracellular stains for FoxP3 (clone 259D/C7, BD Biosciences, RRID:AB_11153143), CTLA-4 (clone BNI3, BD Biosciences, RRID:AB_10893816), Eomes (clone WD1928, eBioscience, RRID:AB_2574616), T-bet (clone 4B10, BioLegend, RRID:AB_2561761), and Ki67 (clone B56, BD Biosciences, RRID:AB_10611571). Permeabilization was performed using the Foxp3 Fixation/ Permeabilization Concentrate and Diluent kit (eBioscience). Cells were resuspended in 1% paraformaldehyde until acquisition on a BD Biosciences LSR II cytometer or Symphony A5 and analyzed using FlowJo (Tree Star).

IHC staining (single chromogenic)

Five micron–thick tissue sections cut from formalin-fixed paraffin-embedded (FFPE) or frozen tissue blocks were used in the study. FFPE tissue blocks were deparaffinized and rehydrated with serial passage through changes of xylene and graded ethanol. FFPE slides were subjected to heat-induced epitope retrieval in ER1 or ER2 solution (Leica Microsystems AR9961 or AR9940). Endogenous peroxidase in tissues was blocked by incubation of slides in 3% hydrogen peroxide solution before incubation with primary antibody (anti-CD45, 1:200, clone 2B11+PD7/26, Agilent, RRID:AB_2314143; anti-CD8, 1:40, clone C8/144B, Agilent, RRID:AB_2075537; anti-CD4, prediluted, clone EP204, Biocare, RRID:AB_3075455; or anti-CD20, prediluted, clone L26, Agilent, RRID:AB_3075456). Staining was performed on a Leica Bond-IIITM instrument using the Bond Polymer Refine Detection System (Leica Microsystems DS9800). Similar procedures were used for frozen tissue sections except antigen retrieval was omitted. Stained slides were counterstained with hematoxylin and cover slipped for review.

Statistical analysis

For patient demographics, medians and ranges were used to summarize continuous variables and percentages were used to summarize categoric variables. Fisher exact test was used for comparison of dichotomous data. Results are indicated as mean ± SD, and *P* values less than 0.05 were considered significant. Receiver operating characteristic (ROC) curves were constructed and the maximum sum of sensitivity and specificity (Youden index) was used to determine the optimal threshold for change in SUV_{max}, with thresholds involving an absolute change of less than 30% excluded due to the known variability in SUV measurements (21). Objective response was defined as a combination of complete response (CR) and partial response (PR). Progression free survival (PFS) was defined as the time from the PET1 scan to progression, according to RECIST 1.1, or death from any cause, whichever occurred first. Patients who remained alive and free from disease progression were censored at last follow-up. Overall survival (OS) was defined as the time from the PET1 scan until death from any cause or last follow-up visit. Patients who remained alive were censored at last follow-up. The data were dichotomized into MF-MR and SM groups, and median PFS and OS were estimated by the Kaplan–Meier method, along with 95% confidence intervals (CI) constructed using the Brookmeyer–Crowley formula. Comparisons of PFS and OS were performed by log-rank test. GraphPad Prism version 9.4.1 (GraphPad Software Inc.) and SPSS version 26 (IBM Corp.) were used for the statistical analyses.

Data availability

The data generated in this study are available within the article and its Supplementary Data files. Deidentified raw data that support the findings of the study are available upon request from the corresponding author.

Results

Patients

Twenty-one patients with advanced melanoma scheduled to initiate pembrolizumab were prospectively enrolled. Two patients who did not complete both PET0 and PET1 were excluded from the analysis. **Table 1** summarizes the patient characteristics, which are listed in Supplementary Table S1. The majority of patients had Eastern Cooperative Oncology Group Performance Status (ECOG PS) 0 (79%), normal LDH level (74%), stage 4 disease (68%), and no prior treatment (84%). In addition, the median baseline tumor burden was 5.0 cm and the majority did not have liver metastases (89%). The representativeness of the study participants is summarized in Supplementary Table S2. PET0 was acquired at a median of 9 days (range, 0–24 days) prior to initiation of pembrolizumab, and PET1 was acquired at a median of 7 days (range, 3–21 days) after the first dose

Table 1. Patient characteristics.

Characteristics	*N* (%)
Median age, years (range)	71 (24–89)
Gender	
Male	14 (74%)
Female	5 (26%)
ECOG PS	
0	15 (79%)
1	4 (21%)
LDH	
Normal	14 (74%)
Elevated	3 (16%)
Missing	2 (11%)
Stage	
3B	2 (11%)
3C	4 (21%)
4	13 (68%)
Liver metastases	
Present	2 (11%)
Absent	17 (89%)
Median baseline tumor burden, cm (range)	5.0 (1.2–18.1)
Treatment history	
None	16 (84%)
Ipilimumab	1 (5%)
Targeted therapy	1 (5%)
Radiotherapy (brain)	1 (5%)

Abbreviation: LDH, lactate dehydrogenase.

of pembrolizumab. The scan intervals for each patient are listed in Supplementary Table S3. PET/CT scans were performed at a median of 60 minutes (range, 52–87 minutes) after FDG injection.

FDG PET/CT response assessment and analysis of peripheral blood

The best overall responses for each patient are included in Supplementary Table S3. 7 patients had a CR, 4 patients had a PR, and 7 patients had progressive disease (PD). One patient had their melanoma completely resected 2 weeks after their PET1 scan and was classified as pathologic nonresponse (pNR), which was treated as PD for the purposes of analysis. No patients had stable disease (SD).

The proposed tumor response to immunotherapy, as measured by FDG PET/CT versus time, is depicted in **Fig. 1A**. Changes in tumor SUV_{max} between PET0 and PET1 ranged from 114% to −70.7% (**Fig. 1B**). ROC analysis revealed that the optimal threshold for a

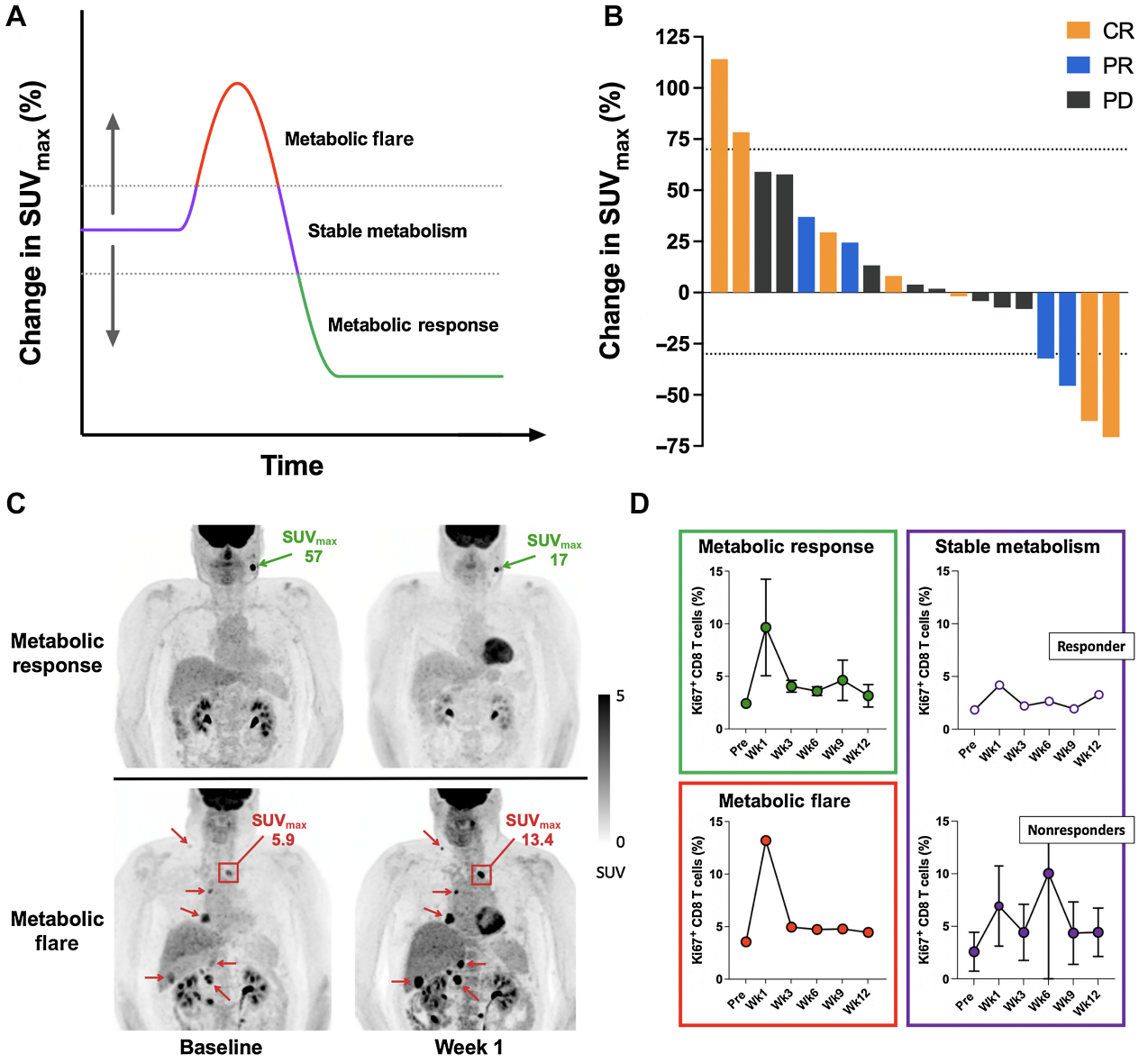

Figure 1.

Early FDG PET/CT predicts response to immunotherapy and is correlated with peripheral blood data. **A,** Schematic of the hypothetical response to cancer immunotherapy, graphed as a function of change in tumor SUV_{max} as measured by FDG PET/CT versus time. Dotted lines represent the threshold for an MF and MR, respectively. **B,** Waterfall plot of change in tumor SUV_{max}, between baseline (PET0) and early post-treatment (PET1) FDG PET/CT scans, according to treatment response. Dotted lines represent +70% and −30% change in SUV_{max}, respectively. **C,** Maximum intensity projection (MIP) FDG PET/CT images of two patients at baseline and 1 week after starting pembrolizumab. Patient 5 (top) had an interval drop in SUV_{max} in a left neck metastasis representative of a metabolic response (change in SUV_{max} = −70.7%). Patient 3 (bottom) had an interval increase in SUV_{max} across multiple lesions representative of a metabolic flare (change in SUV_{max} = 114%). Both patients went on to have a CR to therapy. **D,** Analysis of $Ki67^+$ CD8 T cells in peripheral blood at the indicated times in patients with a metabolic response (patients 4 and 5) and metabolic flare (patient 3), a responding patient with stable metabolism (patient 7), and nonresponding patients with stable metabolism (patients 13–16, 18).

Table 2. Clinical response by PET-defined group.

	N (%) CR/PR	PD/pNR	ORR (%)
All patients	11	8	58%
PET-defined group			
MF-MR	6 (55%)	0 (0%)	100%
SM	5 (45%)	8 (100%)	38%

Note: $P = 0.018$, Fisher exact test.

metabolic flare (MF) was a 70% increase in SUV_{max}, and the optimal threshold for a metabolic response (MR) was a 30% decrease in SUV_{max}. If the change in SUV_{max} did not meet criteria for an MF nor MR, it was classified as stable metabolism (SM). An MF or MR was identified in 6 of 11 (55%) responders and 0 of 8 (0%) nonresponders, with an objective response rate (ORR) of 100% in the MF-MR group and an ORR of 38% in the SM group (**Table 2**). The accuracy was 74%, with a positive predictive value of 100% and negative predictive value of 62%. Responders with either an MF or MR were seen throughout the post-treatment interval, with an MF seen on posttreatment day 6 and 12, and an MR seen on day 7, 8, and 13 (Supplementary Table S3). Representative examples of an MR and MF are provided in **Fig. 1C**. In addition, an exploratory analysis was performed using the largest change in a single FDG-avid tumor lesion for each patient, which provided similar results with two exceptions: one responder (patient 1) previously classified as having SM now had an MF (based on a 122.0% change in SUV_{max} in one lesion), and one nonresponder (patient 15) previously classified as having SM now had an MR (based on a -31.0% change in SUV_{max} in one lesion), suggesting that this approach is a viable alternative and may have greater sensitivity, but it could be subject to more variability and thus might require higher thresholds.

Peripheral blood samples from 9 of 19 (47%) patients were available for analysis. A combined analysis of these samples revealed a robust increase in $Ki67^+$ CD8 T cells that peaked at approximately 1 week post-treatment (at the time of the PET1 scan) and then declined, with responding cells enriched in cells that coexpressed PD-1 and CTLA-4, which we previously reported (with fewer samples) as companion data to a neoadjuvant trial of pembrolizumab in patients with melanoma (17). Further analysis revealed that the largest peaks in $Ki67^+$ CD8 T cells were seen in patients with a MF or MR, while smaller changes in the percentage of $Ki67^+$ CD8 T cells were seen in patients with SM, including both responding and nonresponding patients, although this difference was not significant (**Fig. 1D**; Supplementary Fig. S1). In addition, a moderate correlation was identified between the change in SUV_{max} and percentage of $Ki67^+$ CD8 T cells at the time of PET1 (Supplementary Fig. S2).

One patient that participated in this trial also participated in a phase I imaging trial of a CD8-targeted PET probe, ^{89}Zr-Df-IAB22M2C (^{89}Zr-crefmirlimab berdoxam), at 4 weeks posttreatment (22). In this patient, two groups of metastases demonstrated an MR on the PET1 scan, and were cold on CD8 PET imaging, while a group of metastases in the left upper axilla demonstrated SM on the PET1 scan and were hot on CD8 PET imaging (**Fig. 2A**). These findings suggest that the kinetics of response can vary between lesions in the same patient, and that changes in FDG activity can reflect differences in immune cell infiltration. Variable interlesional response kinetics may also account for the findings in several other responding patients whose metastases demonstrated a wide range of changes in FDG activity across individual lesions, for example from +122.0% to –42.0% SUV_{max} (patient 1) and from +208.9% to –24.1% SUV_{max} (patient 9).

Analysis of early posttreatment tumor biopsies

Two patients had a posttreatment tumor biopsy on the same date as their PET1 scan, and both patients ultimately responded to therapy. In the first patient (patient 5), the posttreatment biopsy (**Fig. 2B**) demonstrated robust infiltration of the tumor by immune cells, which primarily consisted of $CD8^+$ and $CD4^+$ T cells. Necrosis could not be definitively assessed, because morphology on the frozen sections was poorly preserved. Analysis by flow (**Fig. 2C**; Supplementary Fig. S3) revealed that a large percentage of the TILs were T cells, and the majority (75%) were $CD8^+$ T cells that demonstrated an exhausted phenotype and increased Ki67 expression, consistent with recent reinvigoration of T cells by PD-1 blockade followed by exhaustion. Given that this biopsied tumor demonstrated a robust metabolic response on PET1 (with a –70.7% change in SUV_{max}), the data suggest that this lesion is near the end of the response curve (**Fig. 1A**), and is characterized by tumor cell death and exhausted T cells that have impaired glycolysis. In the second patient (patient 9), the posttreatment biopsy (**Fig. 2B**) also demonstrated robust infiltration of the tumor by immune cells, which was significantly increased compared with the baseline biopsy which had no TILs. However, in contrast to the first patient, these TILs primarily consisted of $CD20^+$ B cells, with few T cells. In addition, no necrosis was identified. Analysis by flow (**Fig. 2C**) confirmed that there were very few T cells (0.07%), which were mostly $CD4^+$ and were neither exhausted nor recently activated. Given that this biopsied tumor demonstrated stable metabolism on PET1 (with a +0.2% change in SUV_{max}), the data suggest that this tumor might be at the beginning of the response curve (**Fig. 1A**), although it is also possible that the tumor is just past the peak immune response, or is in the middle of the peak immune response without a metabolic flare.

Identification of new lesions

Two patients demonstrated new FDG-avid lesions on their PET1 scan, which helped to guide their clinical management. In one patient, a brain metastasis was identified on the PET1 scan performed 3 days after starting pembrolizumab (Supplementary Fig. S4A), which was confirmed with MRI and subsequently treated with radiation; this patient went on to have a durable PR. In a second patient, a new FDG-avid splenic lesion was seen on the PET1 scan (Supplementary Fig. S4b), which became more FDG avid on follow-up imaging and correlated with an enhancing lesion on MRI. The splenic lesion was favored to represent pseudoprogression, so the patient continued on therapy, and the lesion resolved on the 6-month FDG PET/CT; this patient went on to have a durable CR.

Change in tumor size

In general, only small changes in tumor size were noted between PET0 and PET1, with small decreases in size more common in responding patients and small increases in size more common in nonresponding patients (Supplementary Table S3). Notably there was essentially no change in tumor size (range: 0 to 1.3%) in patients with a MF, and only mild changes in tumor size (range: -7.7% to 2.9%) in patients with an MR. However, in a few nonresponding patients there were larger increases in tumor size, which were only seen in patients with >10 days between their PET0 scan and start of therapy. In these cases, the tumor had additional time to grow prior to therapy, which likely resulted in increased FDG activity. For example, nonresponding patients who had >10 days between their PET0 scan and treatment

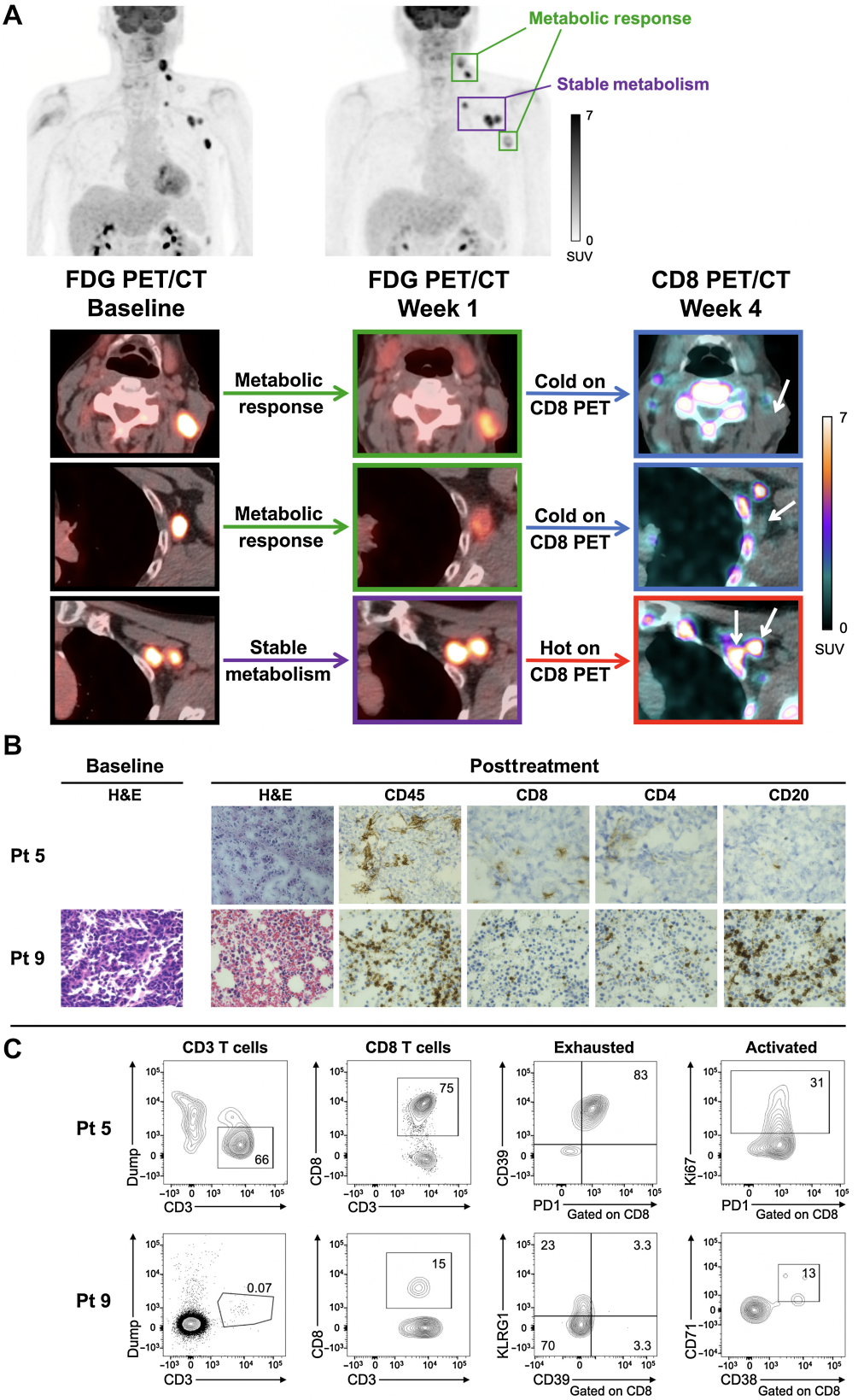
A
Metabolic response
Stable metabolism
7
0
SUV
FDG PET/CT Baseline
FDG PET/CT Week 1
CD8 PET/CT Week 4
Metabolic response
Metabolic response
Stable metabolism
Cold on CD8 PET
Cold on CD8 PET
Hot on CD8 PET
7
0
SUV
B
Baseline
Posttreatment
H&E
H&E
CD45
CD8
CD4
CD20
Pt 5
Pt 9
C
CD3 T cells
CD8 T cells
Exhausted
Activated
Pt 5
Pt 9
Dump
CD3
66
CD8
75
CD39
PD1
83
Ki67
31
Gated on CD8
0.07
15
KLRG1
23
3.3
70
3.3
CD71
13
CD38

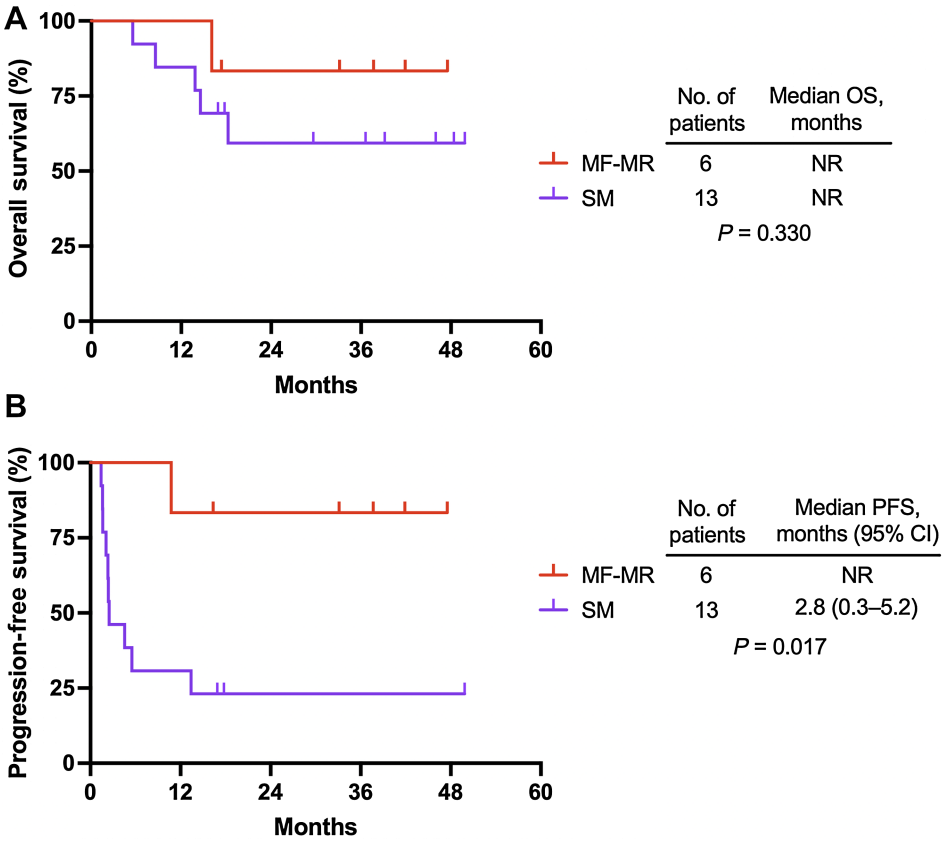

Figure 3.
Early FDG PET/CT is correlated with survival. **A,** Kaplan–Meier estimates of OS stratified by MF-MR and SM groups. **B,** Kaplan–Meier estimates of PFS stratified by MF-MR and SM groups. PFS was assessed according to RECIST v1.1. *P* values were calculated with the log-rank test. OS, overall survival; PFS, progression-free survival; MF-MR, metabolic flare–metabolic response; SM, stable metabolism.

initiation had an average increase in tumor size of 12% ($n = 6$; range: 1.7%–27.3%), and the patient with the largest increase in tumor size (27.3%) had a 59.0% increase in tumor FDG activity.

Given that tumor growth in nonresponding patients could result in increased FDG activity which would resemble an MF in responding patients, a subset of patients was analyzed in which the interval from the PET0 scan to therapy start was restricted to <10 days. In this cohort, in which the confounding effect of tumor growth was reduced, a >30% increase in SUV_{max} was used to define MF, which is in alignment with PERCIST (21). This lower threshold allowed more responders to be captured, including a patient with a 37.0% increase in SUV_{max} on day 14 post-treatment who went on to have a durable PR. In the resulting cohort ($n = 10$; Supplementary Fig. S5), an MF or MR was seen in 6 of 8 (75%) responders and 0 of 2 (0%) nonresponders, with an accuracy of 80%. In this subset of patients, a greater percentage of responders were identified (75% vs. 55%) and the accuracy was similar (80% vs. 74%) compared with the full cohort of patients. Only two patients were misclassified: patient 6, who had a CR with a 29.4% increase in SUV_{max}, which was very close to the 30% threshold for a MF, and patient 2, who had a CR with a -1.8% change in SUV_{max}. For comparison, when this lower threshold was used to analyze the entire cohort, a MF or MR was seen in 7 of 11 (64%) responders and 2 of 8 (25%) nonresponders, with an accuracy of 68%, which may reflect the confounding effect of tumor growth that resulted in a >30% increase in FDG activity in two nonresponding patients.

Survival analysis

Median follow-up was 38 months (range: 17–50 months). At the time of analysis, 6 deaths had occurred; 17% (1/6) of patients had died in the MF-MR group and 38% (5/13) had died in the SM group. Median OS was not reached for either group (**Fig. 3A**). There were 11 PFS events; 1 (17%) in the MF-MR group and 10 (77%) in the SM group. Median PFS was more than 38 months (median not reached) in the MF-MR group versus 2.8 months (95% CI, 0.3–5.2) in the SM group (**Fig. 3B**). PFS was significantly longer in the MF-MR group than in the SM group ($P = 0.017$).

Figure 2.
Correlation of early FDG PET/CT with CD8 PET/CT and tumor biopsies. **A,** Maximum intensity projection (MIP) FDG PET/CT images (top) of patient 4 at baseline and 1 week after starting pembrolizumab, with axial fused FDG PET/CT images (bottom) highlighting specific metastases in the left neck and left axilla, and corresponding axial fused CD8 (^{89}Zr-crefmirlimab berdoxam) PET/CT images (bottom right) at 4 weeks after starting therapy. Although the patient was classified as having a metabolic response (based on changes in SUV_{max} in both target lesions and all lesions), a group of lymph nodes in the left upper axilla demonstrated stable metabolism (average change in $SUV_{max} = 6.2\%$). The metastases that demonstrated a metabolic response on FDG PET/CT (green boxes) were cold on CD8 PET/CT (blue boxes, white arrows), while the metastases that demonstrated stable metabolism on FDG PET/CT (purple boxes) were hot on CD8 PET/CT (red box, white arrows). The patient went on to have a durable CR to therapy. **B,** H&E and IHC staining of CD45, CD8, CD4, and CD20 in tumor biopsies from two responding patients (patients 5 and 9). The posttreatment biopsy was performed on the same day as PET1, after the scan was completed, on day 7 (for patient 5) and on day 12 (for patient 9). The biopsied tumors demonstrated a −70.7% change in SUV_{max} (patient 5) and +0.2% change in SUV_{max} (patient 9) on the PET1 scan. **C,** Representative flow plots of posttreatment tumor samples from patient 5 and patient 9.

Discussion

This is the first study, to our knowledge, that has explored the early metabolic changes in tumor lesions using FDG PET/CT at approximately 1 week after starting anti–PD-1 therapy. In this study, we confirmed that an MF and MR can both occur within days following treatment with anti–PD-1 therapy, and demonstrated that those changes in tumor FDG activity are predictive of response and are significantly correlated with PFS in patients with advanced melanoma. Previous reports of interim FDG PET/CT imaging in the setting of cancer immunotherapy have typically imaged patients after 3–4 weeks of therapy, and more commonly after 6 weeks, at which point increases in FDG activity due to response (frequently termed pseudoprogression) cannot be discriminated from increases in FDG activity due to true progression (14–16, 23–31). In contrast, our approach to image patients about 1 week after starting therapy minimizes tumor growth, and restricts changes in FDG activity to responding patients, which were identified in this limited pilot study with 100% specificity.

Early response assessment has several advantages, including the potential to enable personalized treatment of patients on cancer immunotherapy. The early identification of nonresponding patients allows treatment to be escalated, or alternative therapies to be given earlier, which could improve outcomes and reduce unnecessary side effects from ineffective therapy. In addition, the early identification of responding patients could potentially enable de-escalation of therapy, for example by reducing or avoiding surgery, much like a major pathologic response was used as a criterion for surgical de-escalation in the PRADO trial, which could decrease morbidity and increase quality of life (32). Responding patients could also de-escalate from combination immunotherapy to monotherapy, using an approach similar to the ADAPT-IT trial, although it appears that most of the toxicity of immunotherapy is built into the first two doses, making this approach less attractive (33). The early identification of occult metastases or immune-related lesions could also help to stage patients, inform their clinical management, and better identify pseudoprogression on subsequent studies. In the current study, two patients demonstrated new lesions on early FDG PET/CT imaging that helped to guide their clinical management. The first patient had a brain metastasis that was identified on early FDG PET/CT imaging, which enabled the metastasis to be treated with radiation, and the patient went on to have a durable response. The second patient had a new splenic lesion that was seen on early FDG PET/CT imaging, which allowed it to be classified as pseudoprogression on subsequent imaging.

We hypothesize that the response to immunotherapy, as measured by changes in tumor FDG activity, begins with an MF and is followed by an MR, which reflects an initial influx of activated tumor-infiltrating immune cells that is followed by significant tumor cell death and exhaustion/clearance of immune cells (**Fig. 1A**). On the basis of this proposed response curve, there are two time points when a responding patient will have SM: prior to the initiation of response, and at the inflection point when a tumor lesion is moving from an MF to an MR. However, more research is needed to test this hypothesis, and to better understand the kinetics of response. In this study, the data show that the kinetics of response are rapid but vary between patients, with an MF seen on day 6 and day 12, and an MR seen on day 7, day 8, and day 13. In addition, a patient who participated in both FDG and CD8 PET imaging trials demonstrated that there is variability in the kinetics of response between lesions within the same patient, and that changes in FDG activity can correlate with differences in CD8 T-cell infiltration. Several metastases in this patient had a drop in FDG activity on the PET1 scan consistent with an MR, and were cold on CD8 PET, suggesting that the lesions had nearly finished responding. In contrast, several other metastases had SM, and were hot on CD8 PET, suggesting that they had CD8 T cells present and may have been at the inflection point between an MF and MR with a balanced degree of immune cell infiltration and tumor cell death, or alternatively at the beginning of the response curve. Given this variability in response kinetics, we anticipate that the presence of at least one metastatic lesion with an unambiguous MF or MR will likely be enough to predict response, and may have greater sensitivity than a summed measure of more than one lesion. This is supported by an exploratory analysis of the imaging data in this trial that used the largest change in a single lesion to predict response, which provided similar results. However, the variability in response kinetics also makes it unlikely that a single posttreatment scan will be capable of identifying all responders and nonresponders with 100% sensitivity and specificity. Instead, we anticipate a scenario in which early FDG PET/CT imaging could be used to identify a set of responders with confidence, based on a MF or MR, and then the cohort with SM that is enriched in nonresponders would proceed to have additional imaging studies, or complementary biomarkers measured, to correctly identify all of the responders and nonresponders within the cohort.

Our data identified both an MF and MR as indicators of response to immunotherapy. Additional evidence that an MF and MR serve as related measures of response comes from the peripheral blood data, in which large increases in $Ki67^+$ CD8 T cells were seen in patients with both an MF and an MR, which was larger than the increase in $Ki67^+$ CD8 T cells in nonresponding patients with SM. These data also suggest that there is a temporal correlation between changes in tumor FDG activity and reinvigoration of CD8 T cells in the peripheral blood. In addition, some responding patients demonstrated SM, and had a blunted increase in $Ki67^+$ CD8 T cells in the peripheral blood, suggesting that the imaging time point (and paired blood draw) missed the peak immune response, again underscoring the variability in the timing of the immune response across patients. However, it is also possible that these responding patients with SM never mounted a measurable response to immunotherapy. Additional data were provided by early posttreatment tumor biopsies in two patients, who ultimately responded to therapy. In one patient the biopsy demonstrated an abundance of recently proliferating exhausted CD8 T cells, which are known to have impaired glycolysis (34, 35), and was consistent with the observed MR in the biopsied tumor. In the other patient the biopsy demonstrated robust infiltration of the tumor with B cells, and very few T cells, suggestive of the development of tertiary lymphoid structures within the tumor, which have been associated with response to immunotherapy (36, 37). Given that this tumor demonstrated SM on the PET1 scan, it is not clear if the lesion was imaged and biopsied at an early or late point along the response curve, or how the B cells affected the overall metabolism of the lesion. Thus, additional research is needed to better understand the patterns of response to immunotherapy at early time points, the impact of those responses on overall tumor metabolism, and the relationship between changes in tumor FDG activity and changes in immune cell populations in the peripheral blood.

This study used a threshold of >70% increase in SUV_{max} to define a MF. However, we anticipate that a lower threshold might be able to be used for subsequent studies if the time between PET0 and initiation of therapy is minimized, to limit the impact of tumor growth on the analysis. To support this approach, a subset of patients was analyzed in which this interval was kept to <10 days. In this cohort, a greater

number of responders were identified using a lower threshold of >30% increase in SUV_{max}, with similar accuracy.

This study explored the ability of early FDG PET/CT to predict response in patients with advanced melanoma on anti–PD-1 therapy, but we expect that this approach could also be applied to other cancers and immunotherapy regimens, including cellular therapy, which result in tumor infiltration by activated immune cells. Additional support for the utility of an early FDG PET/CT scan to predict response to anti–PD-1 therapy is provided by data from two recent clinical trials. In one trial, 25 patients with non–small cell lung cancer (NSCLC) treated with nivolumab were imaged with FDG PET/MRI at baseline and at 2 weeks posttreatment (38). In this study, two patients with the largest increase in SUV_{max} (+60%) and the largest decrease in SUV_{max} (−74%) both had a response to therapy, supporting the ability of an MF or MR to predict response in NSCLC. In another recent trial, 10 patients with metastatic melanoma treated with pembrolizumab or nivolumab were imaged with FDG PET/CT and FDG PET/MRI at baseline and at 2 weeks posttreatment (39). In this trial, all three patients with a subsequent complete metabolic response to therapy had a >30% decrease in tumor FDG activity at 2 weeks, supporting the ability of an MR to predict response; no cases of an MF were identified in this trial.

This study is limited by a relatively small sample size from a single institution, which did not include patients with SD. Moreover, there was an objective response in 58% of patients, which is higher than the ORRs reported in other trials of pembrolizumab monotherapy and may have been due to a greater proportion of patients having ECOG PS of 0, normal LDH, an absence of liver metastases, and low volume disease compared with prior studies (20, 40). Further, there were variable intervals between PET0 and therapy initiation, and between therapy initiation and PET1 (with considerable variation from the target interval of 1 week), which informed the variable kinetics of response and confirmed that baseline scans should be acquired as close to therapy start as possible; however, future studies will need to define these intervals more narrowly. In addition, only two examples of an MF were identified. This study also used a clinical FDG PET/CT protocol, so four different PET/CT scanners were used, which could have caused variability in SUV measurements. Despite this variability, we still observed that an MF or MR was predictive of response, and strongly correlated with PFS, suggesting that response assessment by early FDG PET/CT is robust. However, given the evolving landscape of first-line therapy for advanced melanoma in which the majority of patients are currently treated with combination immunotherapy, we expect that this approach will require validation across additional immunotherapy regimens, including combination therapies, prior to clinical application in the neoadjuvant or metastatic setting.

Authors' Disclosures

A.C. Huang reports personal fees from Immunai and other support from Merck and BMS outside the submitted work. S. McGettigan reports personal fees from Merck, Bristol Myers Squibb, and Regeneron outside the submitted work. E.J. Wherry reports personal fees from Arsenal Bioscience, Coherus, Synthekine, Marengo Therapeutics, Pluto Immunotherapeutics, Santa Ana Bio, Janssen, and New Limit outside the submitted work. R.K. Amaravadi reports other support from Pinpoint Therapeutics; personal fees from Tasca Therapeutics; and grants from Merck, BMS, Springworks, Deciphera, Pfizer, and Novartis outside the submitted work. T.C. Mitchell reports grants and personal fees from BMS and Merck; grants from Incyte; and personal fees from Pfizer and Pliant outside the submitted work. M.D. Farwell reports grants from Merck and grants and personal fees from ImaginAb during the conduct of the study as well as grants from BMS and Carisma and personal fees from Abcuro outside the submitted work. No disclosures were reported by the other authors.

Authors' Contributions

T.M. Anderson: Data curation, formal analysis, validation, investigation, visualization, writing–original draft, writing–review and editing. **B.H. Chang:** Data curation, formal analysis, validation, investigation, visualization, writing–original draft, writing–review and editing. **A.C. Huang:** Resources, data curation, formal analysis, supervision, funding acquisition, validation, investigation, visualization, methodology, writing–original draft, writing–review and editing. **X. Xu:** Resources, formal analysis, validation, investigation, visualization, methodology, writing–original draft, writing–review and editing. **D. Yoon:** Data curation, formal analysis, validation, investigation, visualization, writing–review and editing. **C.G. Shang:** Data curation, formal analysis, validation, investigation, writing–review and editing. **R. Mick:** Formal analysis, visualization, methodology, writing–review and editing. **E. Schubert:** Resources, data curation, supervision, investigation, project administration, writing–review and editing. **S. McGettigan:** Resources, writing–review and editing. **K. Kreider:** Resources, writing–review and editing. **W. Xu:** Resources, project administration, writing–review and editing. **E.J. Wherry:** Resources, supervision, funding acquisition, methodology, writing–review and editing. **L.M. Schuchter:** Resources, writing–review and editing. **R.K. Amaravadi:** Resources, writing–review and editing. **T.C. Mitchell:** Resources, writing–review and editing. **M.D. Farwell:** Conceptualization, resources, data curation, formal analysis, supervision, funding acquisition, validation, investigation, visualization, methodology, writing–original draft, project administration, writing–review and editing.

Acknowledgments

This work was supported by a research grant from the Investigator-Initiated Studies Program of Merck Sharp & Dohme LLC (to M.D. Farwell). The opinions expressed in this paper are those of the authors and do not necessarily represent those of Merck Sharp & Dohme LLC. Clinical and correlative studies were also supported by a research grant from ImaginAb (to M.D. Farwell), the SPORE in Skin Cancer: P50-CA174523 (to X. Xu, L.M. Schuchter, R.K. Amaravadi, R. Mick), P01-CA114046 (to X. Xu), T32-CA009615 and K08-CA230157 (to A.C. Huang), RSNA Resident Research Award and T32-EB004311 (to B.H. Chang), the NIH/NCI Cancer Center Support Grant P30-CA016520 (to R.K. Amaravadi, L.M. Schuchter, R. Mick), NIH grants R01-AI105343, P01-AI108545, U19-AI117950, U19-AI082630, P01-CA210944 (to E.J. Wherry), the Tara Miller Melanoma Foundation (to A.C. Huang), the Melanoma Research Alliance (to E.J. Wherry), the David and Hallee Adelman Immunotherapy Research Fund (to E.J. Wherry), and the Parker Institute for Cancer Immunotherapy Bridge Scholar Award (to A.C. Huang). The Human Immunology Core and the Tumor Tissue and Biospecimen Bank of the University of Pennsylvania (supported by P30-CA016520) assisted in tissue collection, processing, and storage.

The publication costs of this article were defrayed in part by the payment of publication fees. Therefore, and solely to indicate this fact, this article is hereby marked "advertisement" in accordance with 18 USC section 1734.

Note

Supplementary data for this article are available at Clinical Cancer Research Online (http://clincancerres.aacrjournals.org/).

Received August 14, 2023; revised October 31, 2023; accepted December 19, 2023; published first January 24, 2024.

References

1. Larkin J, Chiarion-Sileni V, Gonzalez R, Grob JJ, Cowey CL, Lao CD, et al. Combined nivolumab and ipilimumab or monotherapy in untreated melanoma. N Engl J Med 2015;373:23–34.
2. Marrone KA, Ying W, Naidoo J. Immune-related adverse events from immune checkpoint inhibitors. Clin Pharmacol Ther 2016;100:242–51.
3. Kornberg MD. The immunologic Warburg effect: evidence and therapeutic opportunities in autoimmunity. Wiley Interdiscip Rev Syst Biol Med 2020;12:e1486.
4. Patsoukis N, Bardhan K, Chatterjee P, Sari D, Liu B, Bell LN, et al. PD-1 alters T-cell metabolic reprogramming by inhibiting glycolysis and promoting lipolysis and fatty acid oxidation. Nat Commun 2015;6:6692.

5. Kubota R, Yamada S, Kubota K, Ishiwata K, Tamahashi N, Ido T. Intratumoral distribution of fluorine-18-fluorodeoxyglucose in vivo: high accumulation in macrophages and granulation tissues studied by microautoradiography. J Nucl Med 1992;33:1972–80.
6. Nair-Gill E, Wiltzius SM, Wei XX, Cheng D, Riedinger M, Radu CG, et al. PET probes for distinct metabolic pathways have different cell specificities during immune responses in mice. J Clin Invest 2010;120:2005–15.
7. Reinfeld BI, Madden MZ, Wolf MM, Chytil A, Bader JE, Patterson AR, et al. Cell-programmed nutrient partitioning in the tumour microenvironment. Nature 2021;593:282–8.
8. Casali M, Lauri C, Altini C, Bertagna F, Cassarino G, Cistaro A, et al. State of the art of (18)F-FDG PET/CT application in inflammation and infection: a guide for image acquisition and interpretation. Clin Transl Imaging 2021;9: 299–339.
9. Burger IA, Husmann L, Hany TF, Schmid DT, Schaefer NG. Incidence and intensity of F-18 FDG uptake after vaccination with H1N1 vaccine. Clin Nucl Med 2011;36:848–53.
10. Kubota K, Saginoya T, Ishiwata K, Nakasato T, Munechika H. [(18)F]FDG uptake in axillary lymph nodes and deltoid muscle after COVID-19 mRNA vaccination: a cohort study to determine incidence and contributing factors using a multivariate analysis. Ann Nucl Med 2022;36:340–50.
11. Gandy N, Arshad MA, Wallitt KL, Dubash S, Khan S, Barwick TD. Immuno-therapy-related adverse effects on (18)F-FDG PET/CT imaging. Br J Radiol 2020; 93(1111):20190832.
12. Escuin-Ordinas H, Elliott MW, Atefi M, Lee M, Ng C, Wei L, et al. PET imaging to non-invasively study immune activation leading to antitumor responses with a 4–1BB agonistic antibody. J Immunother Cancer 2013;1:14.
13. Chargari C, Le Moulec S, Bonardel G, Foehrenbach H, Vedrine L. Ipilimumab in cancer patients: the issue of early metabolic response. Anticancer Drugs 2013;24: 324–6.
14. Sachpekidis C, Larribere L, Pan L, Haberkorn U, Dimitrakopoulou-Strauss A, Hassel JC. Predictive value of early 18F-FDG PET/CT studies for treatment response evaluation to ipilimumab in metastatic melanoma: preliminary results of an ongoing study. Eur J Nucl Med Mol Imaging 2015;42:386–96.
15. Cho SY, Lipson EJ, Im HJ, Rowe SP, Gonzalez EM, Blackford A, et al. Prediction of response to immune checkpoint inhibitor therapy using early-time-point (18) F-FDG PET/CT imaging in patients with advanced melanoma. J Nucl Med 2017; 58:1421–8.
16. Sachpekidis C, Kopp-Schneider A, Hassel JC, Dimitrakopoulou-Strauss A. Assessment of early metabolic progression in melanoma patients under immu-notherapy: an (18)F-FDG PET/CT study. EJNMMI Res 2021;11:89.
17. Huang AC, Orlowski RJ, Xu X, Mick R, George SM, Yan PK, et al. A single dose of neoadjuvant PD-1 blockade predicts clinical outcomes in resectable melanoma. Nat Med 2019;25:454–61.
18. Kim KH, Cho J, Ku BM, Koh J, Sun JM, Lee SH, et al. The first-week proliferative response of peripheral blood PD-1(+)CD8(+) T cells predicts the response to anti-PD-1 therapy in solid tumors. Clin Cancer Res 2019;25:2144–54.
19. Eisenhauer EA, Therasse P, Bogaerts J, Schwartz LH, Sargent D, Ford R, et al. New response evaluation criteria in solid tumours: revised RECIST guideline (version 1.1). Eur J Cancer 2009;45:228–47.
20. Joseph RW, Elassaiss-Schaap J, Kefford R, Hwu WJ, Wolchok JD, Joshua AM, et al. Baseline tumor size is an independent prognostic factor for overall survival in patients with melanoma treated with pembrolizumab. Clin Cancer Res 2018; 24:4960–7.
21. Wahl RL, Jacene H, Kasamon Y, Lodge MA. From RECIST to PERCIST: evolving considerations for PET response criteria in solid tumors. J Nucl Med 2009;50 Suppl 1(Suppl 1):122S–50S.
22. Farwell MD, Gamache RF, Babazada H, Hellmann MD, Harding JJ, Korn R, et al. CD8-targeted PET imaging of tumor-infiltrating T cells in patients with cancer: a Phase I first-in-humans study of (89)Zr-Df-IAB22M2C, a radiolabeled anti-CD8 minibody. J Nucl Med 2022;63:720–6.
23. Anwar H, Sachpekidis C, Winkler J, Kopp-Schneider A, Haberkorn U, Hassel JC, et al. Absolute number of new lesions on (18)F-FDG PET/CT is more predictive of clinical response than SUV changes in metastatic melanoma patients receiving ipilimumab. Eur J Nucl Med Mol Imaging 2018;45:376–83.
24. Iravani A, Osman MM, Weppler AM, Wallace R, Galligan A, Lasocki A, et al. FDG PET/CT for tumoral and systemic immune response monitoring of advanced melanoma during first-line combination ipilimumab and nivolumab treatment. Eur J Nucl Med Mol Imaging 2020;47:2776–86.
25. Ito K, Teng R, Schoder H, Humm JL, Ni A, Michaud L, et al. (18)F-FDG PET/CT for monitoring of ipilimumab therapy in patients with metastatic melanoma. J Nucl Med 2019;60:335–41.
26. Nakamoto R, Zaba LC, Rosenberg J, Reddy SA, Nobashi TW, Davidzon G, et al. Prognostic value of volumetric PET parameters at early response evaluation in melanoma patients treated with immunotherapy. Eur J Nucl Med Mol Imaging 2020;47:2787–95.
27. Nobashi T, Baratto L, Reddy SA, Srinivas S, Toriihara A, Hatami N, et al. Predicting response to immunotherapy by evaluating tumors, lymphoid cell-rich organs, and immune-related adverse events using FDG-PET/CT. Clin Nucl Med 2019;44:e272–e9.
28. Sachpekidis C, Anwar H, Winkler J, Kopp-Schneider A, Larribere L, Haberkorn U, et al. The role of interim (18)F-FDG PET/CT in prediction of response to ipilimumab treatment in metastatic melanoma. Eur J Nucl Med Mol Imaging 2018;45:1289–96.
29. Sachpekidis C, Kopp-Schneider A, Pan L, Papamichail D, Haberkorn U, Hassel JC, et al. Interim [(18)F]FDG PET/CT can predict response to anti-PD-1 treatment in metastatic melanoma. Eur J Nucl Med Mol Imaging 2021;48: 1932–43.
30. Schweighofer-Zwink G, Manafi-Farid R, Kolblinger P, Hehenwarter L, Harsini S, Pirich C, et al. Prognostic value of 2-[(18)F]FDG PET-CT in metastatic melanoma patients receiving immunotherapy. Eur J Radiol 2022;146:110107.
31. Vermeulen S, Awada G, Keyaerts M, Neyns B, Everaert H. Early reassessment of total metabolic tumor volume on FDG-PET/CT in advanced melanoma patients treated with pembrolizumab predicts long-term outcome. Curr Oncol 2021;28: 1630–40.
32. Reijers ILM, Menzies AM, van Akkooi ACJ, Versluis JM, van den Heuvel NMJ, Saw RPM, et al. Personalized response-directed surgery and adjuvant therapy after neoadjuvant ipilimumab and nivolumab in high-risk stage III melanoma: the PRADO trial. Nat Med 2022;28:1178–88.
33. Postow MA, Goldman DA, Shoushtari AN, Betof Warner A, Callahan MK, Momtaz P, et al. Adaptive dosing of nivolumab + ipilimumab immunotherapy based upon early, interim radiographic assessment in advanced melanoma (the ADAPT-IT study). J Clin Oncol 2022;40:1059–67.
34. Bengsch B, Johnson AL, Kurachi M, Odorizzi PM, Pauken KE, Attanasio J, et al. Bioenergetic insufficiencies due to metabolic alterations regulated by the inhib-itory receptor PD-1 are an early driver of CD8(+) T cell exhaustion. Immunity 2016;45:358–73.
35. Reina-Campos M, Scharping NE, Goldrath AW. CD8(+) T cell metabolism in infection and cancer. Nat Rev Immunol 2021;21:718–38.
36. Cabrita R, Lauss M, Sanna A, Donia M, Skaarup Larsen M, Mitra S, et al. Tertiary lymphoid structures improve immunotherapy and survival in melanoma. Nature 2020;577:561–5.
37. Helmink BA, Reddy SM, Gao J, Zhang S, Basar R, Thakur R, et al. B cells and tertiary lymphoid structures promote immunotherapy response. Nature 2020; 577:549–55.
38. Umeda Y, Morikawa M, Anzai M, Ameshima S, Kadowaki M, Waseda Y, et al. Predictive value of integrated (18)F-FDG PET/MRI in the early response to nivolumab in patients with previously treated non-small cell lung cancer. J Immunother Cancer 2020;8:e000349.
39. Seith F, Forschner A, Schmidt H, Pfannenberg C, Guckel B, Nikolaou K, et al. 18F-FDG-PET detects complete response to PD1-therapy in melanoma patients two weeks after therapy start. Eur J Nucl Med Mol Imaging 2018;45:95–101.
40. Robert C, Ribas A, Schachter J, Arance A, Grob JJ, Mortier L, et al. Pembro-lizumab versus ipilimumab in advanced melanoma (KEYNOTE-006): post-hoc 5-year results from an open-label, multicentre, randomised, controlled, phase 3 study. Lancet Oncol 2019;20:1239–51.